

Supporting Information

Friction and Work Function Oscillatory Behavior for Even and Odd Number of Layers in Polycrystalline MoS₂

Francesco Lavini^{1,2,3†}, Annalisa Calò^{1,3†}, Yang Gao¹, Edoardo Albisetti^{1,4}, Tai-De Li¹, Tengfei Cao^{2,5}, Guoqing Li⁶, Linyou Cao^{6,7}, Carmela Aruta^{1,8*}, and Elisa Riedo^{1,2,3,9*}

¹Advanced Science Research Center, City University of New York, 85 St Nicholas Terrace, New York, New York 10031, USA

²CUNY Graduate Center, Ph.D. Program in Physics and Chemistry, New York, NY 10016

³Tandon School of Engineering, NYU, New York, NY

⁴Dipartimento di Fisica, Politecnico di Milano, Via Giuseppe Colombo 81, 20133, Milano, Italy

⁵Department of Chemistry, College of Staten Island, City University of New York, 2800 Victory Boulevard, Staten Island, New York 10314, USA

⁶Department of Materials Science and Engineering, North Carolina State University, Raleigh, NC 27695

⁷Department of Physics, North Carolina State University, Raleigh, NC 27695

⁸National Research Council CNR-SPIN, Viale del Politecnico 1, I-00133, Rome, Italy

⁹Physics Department, City College of New York, City University of New York, Marshak Science Building, 160 Convent Avenue, New York, New York 10031, USA

* Corresponding author: elisa.riedo@nyu.edu, carmela.aruta@spin.cnr.it

† These authors contribute equally to this work.

Raman spectroscopy, AFM and STEM of polycrystalline MoS₂

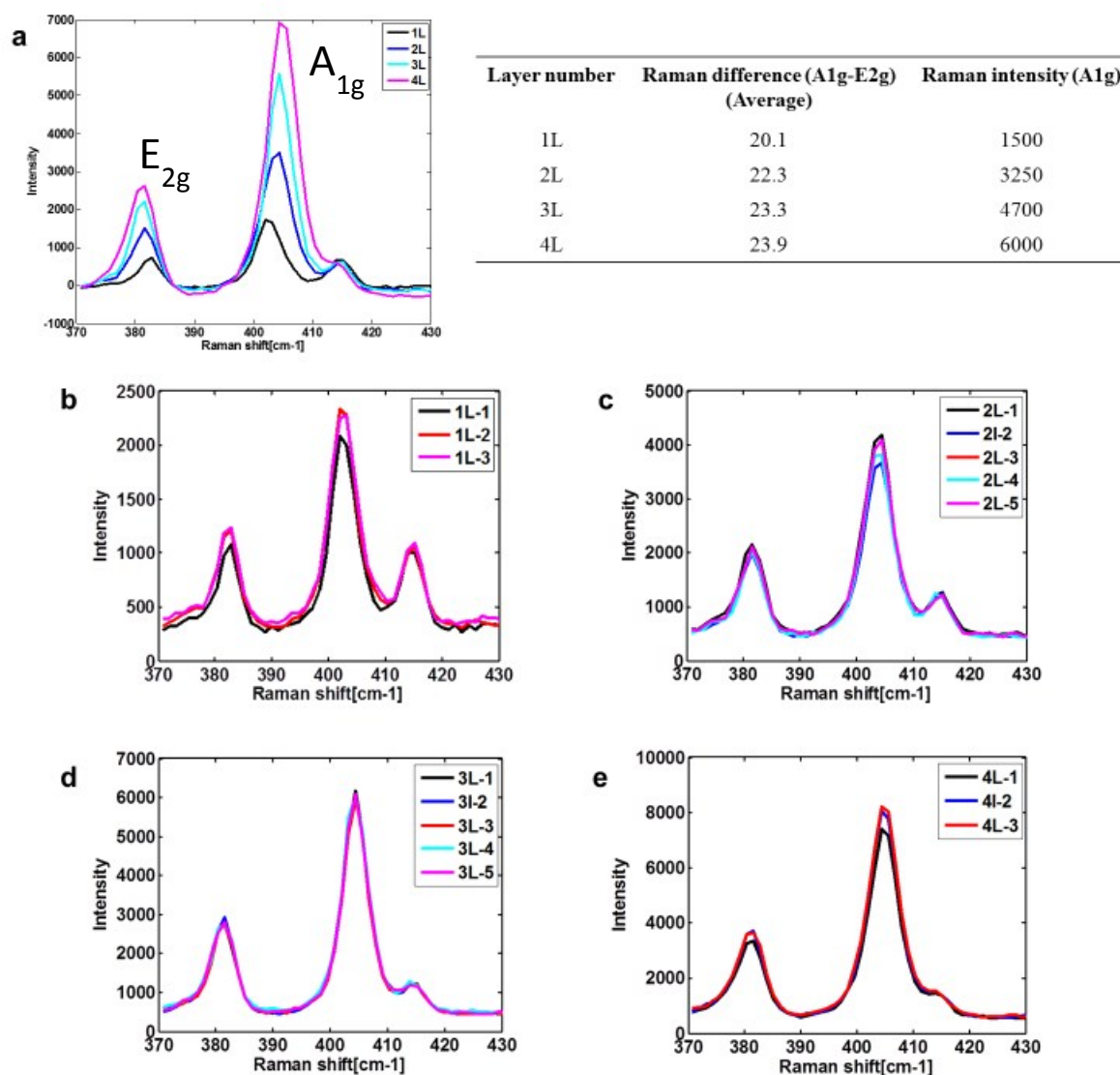


Figure S1. Raman spectroscopy of polycrystalline MoS₂. Raman spectroscopy is used to verify crystalline quality and thickness of the four MoS₂ polycrystalline samples. (a) Average Raman spectra collected from different positions on polycrystalline samples (1L, 2L, 3L, 4L). The table reports the corresponding values of the frequency difference between the A_{1g} and the E_{2g} peaks. This difference is directly related to the thickness of the films, and measured values agree with literature data¹. Also the intensity of the A_{1g} peak is reported for the different films thickness. (b-e) Individual Raman spectra, collected at several positions, for all films (1 to 4 layers respectively). They show the uniformity of the films growth.

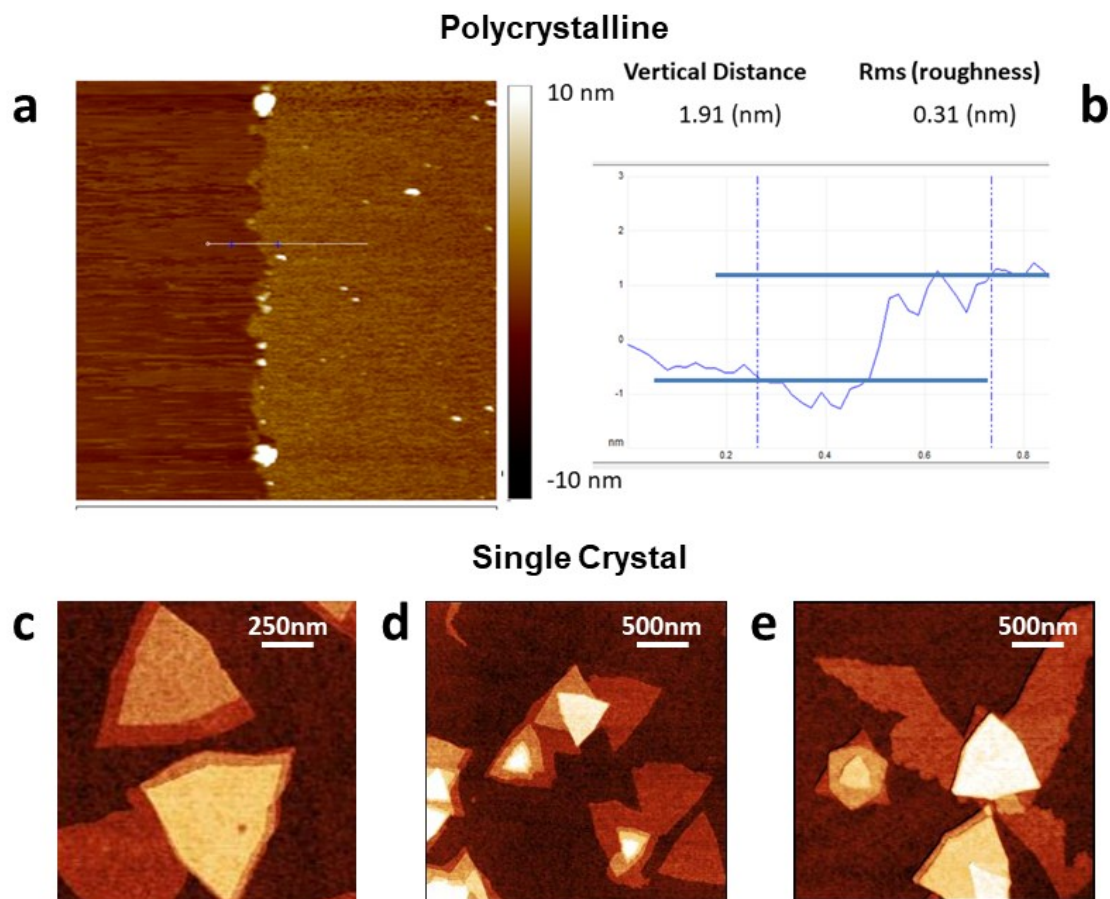


Figure S2. Topography and roughness of polycrystalline and single crystal MoS₂. (a) Contact-mode AFM image of polycrystalline MoS₂ (3L). The height profile (b) corresponding to the white line (x axis indicates the lateral size and y axis the topographic height) confirms film thickness. AFM image size is 2.5 μm. (c, d, e) Contact-mode AFM topographic images of single crystal MoS₂, taken from three different areas on the sample surface. It is possible to identify single crystals of different thicknesses. Images have all same vertical scale (z = 3nm), while respective lateral scale is indicated in each individual image.

Layer number	Thickness (nm) ± 0.05	Roughness (nm) ± 0.02
1L	0.71	0.17
2L	1.36	0.17
3L	1.96	0.28
4L	2.66	0.29

Table S1. Average thickness and roughness of MoS₂ polycrystalline samples. Values are obtained from AFM topography images collected in contact-mode (5 x 5 μm², 256 x 256 pixels, scan rate: 1 Hz).

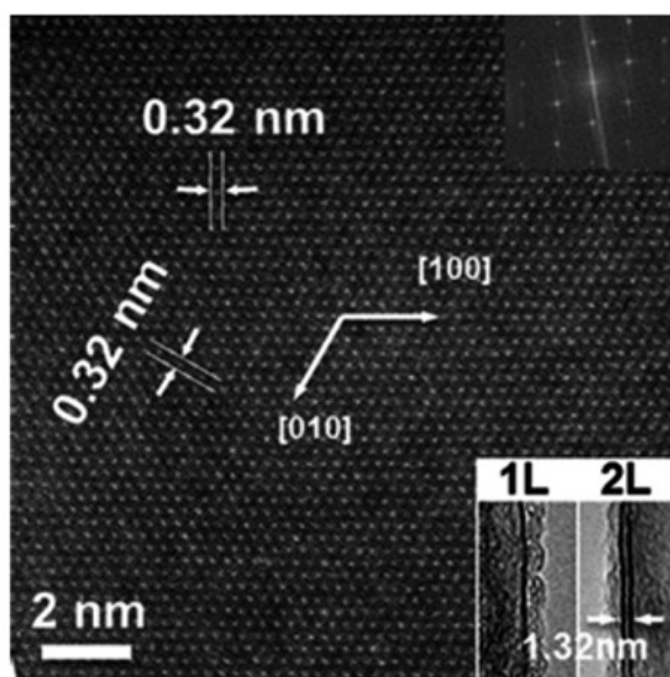


Figure S3. STEM high-angle annular dark field (HAADF) image of MoS₂ films. Lattice constants and relevant crystalline directions are highlighted. Upper inset: corresponding Fast Fourier Transform (FFT) pattern. Lower inset: folded edges of MoS₂ mono- and bilayer films.

Friction Force Microscopy (FFM)

Cantilevers spring constants are calibrated using the thermal noise method², after having measured the optical sensitivity (in nm/V) from the slope of AFM force-distance curves obtained on a bare reference silicon substrate. Lateral spring constants are calibrated considering the lateral force response of the cantilever as it scans across a silicon sample. Typically, atomic scale stick-slip behavior is preceded by an initial sticking portion, the slope of which corresponds to the lateral stiffness, $dF_l/dx = k_l^3$. We verified the experimental results are in agreement with the theoretical estimate, in which the lateral force constant is calculated from beam mechanics using elasticity theory⁴. It requires accurate knowledge of the tip/cantilever dimensions and of the cantilever shear modulus, according to the following Equation:

$$k_l = \frac{Gwt^3}{3l\left(h + \frac{t}{2}\right)^2} \quad (1)$$

where G is the shear modulus of silicon, w , t and l are respectively the width, thickness and length of the cantilever, and h is the tip height. Nominal values for cantilever and tip are used.

Adhesion forces from linear and power law fitting

Previous studies⁵ have demonstrated that for single asperity contacts friction forces F_F may increase with normal load F_N and adhesion forces F_{adh} according to the following Equation:

$$F_F \approx \mu_0 (F_N + F_{adh})^{2/3} \quad (\text{S2})$$

where μ_0 is a parameter with function and meaning similar to the linear friction coefficient μ . Fitting the friction vs. normal load data with Equation S2, we obtain adhesion forces as previously done with the linear fitting. Data are reported in Table S2. We notice that absolute values are lower compared to those obtained from the linear fit (Table S3).

	Polycrystalline	Single Crystal
	F_{adh} (nN)	F_{adh} (nN)
1L	14 ± 1	16 ± 4
2L	33 ± 5	14 ± 9
3L	32 ± 1	21 ± 12
4L	24 ± 4	23 ± 12
Bulk	51 ± 18	51 ± 18

Table S2. Adhesion Forces F_{adh} , and corresponding standard deviation, as a function of number of layers, for polycrystalline and single crystal MoS₂ samples, fitted according to 2/3 equation S2.

	Polycrystalline	Single Crystal
	F_{adh} (nN)	F_{adh} (nN)
1L	25 ± 1	38 ± 6
2L	56 ± 7	37 ± 14
3L	53 ± 2	47 ± 18
4L	41 ± 6	42 ± 18
Bulk	82 ± 29	82 ± 29

Table S3. Adhesion Forces as a function of number of layers, for polycrystalline and single crystal MoS₂, fitted according to the linear Eq. 1 in the main manuscript.

XPS spectroscopy

For XPS measurements we use a Physical Electronics VersaProbe II, with ultra-high vacuum compatibility (UHV pressure $< 10^{-6}$ Pa). The sample is mounted on a steel sample holder and grounded. The analyzer acceptance angle was 20° , the take-off angle was 45° , and pass energy was 11.75 eV (Mo $3d$ and S $2p$) and 46.95 eV (valence band). We collect Mo $3d$, S $2p$ and O $1s$ core level and valence band (VB) spectra on polycrystalline MoS₂ samples. Binding energy (BE) calibration is performed with reference to the Al $2p$ peak from the sapphire substrate. The fitting procedure of the core levels is performed while keeping fixed as much as possible the fitting parameters. For all the spectra a Shirley function is assumed for background subtraction and a multicomponent deconvolution procedure, using mixed Gaussian and Lorentzian line shapes. The results for Mo $3d$ and S $2p$ are reported in Fig. S4. The spectra in Fig. S4 a and b show the typical fitting results for 1L polycrystalline MoS₂. For the Mo $3d$ (Fig. S4a) we use two couples of $3d_{5/2}$ and $3d_{3/2}$ spin-orbit doublets for the Mo⁴⁺ and Mo⁶⁺ valence states. In the fitting procedure the chemical shift between Mo⁴⁺ and Mo⁶⁺ is fixed at 2.96 eV, the spin orbit splitting fixed at 3.14 eV, the degeneracy ratio is 2:3 for the spin-orbit area ratio and the full width at half maximum (FWHM) is a free parameter but fixed at the same value for the two peaks of each doublet. For the S $2p$ (Fig. S4b) we also use the minimum number of components to fit the doublet of the $2p_{3/2}$ and $2p_{1/2}$ spin-orbit splitting. The splitting is fixed at 1.2 eV, the degeneracy ratio is 1:2 for the spin-orbit area ratio and the FWHM is a free parameter but the same for both peaks. On the other hand, we know that MoS₂ single crystals analyzed in our study have a characteristic dimension of around 1 μm and the distribution and density of the crystals on the surface of the sample is such that crystals of different, random thickness are found within the same micrometer-size area. The lateral spatial resolution of the XPS experimental set-up used here, which is around 200 μm , does not allow to select regions with only a single defined population of thickness. In Fig. S4c and Fig. S4d we report the Mo $3d$ and S $2p$ core levels spectra of single crystals MoS₂, with a variety of thicknesses, see for example Fig. S2. The asymmetry of the peaks indicates contribution from layers thicker than one. The fitting procedure of the single crystal core levels is performed similarly to the case of the polycrystalline samples but using an extra doublet at lower BE, which should be considered a convolution of contributions from crystals of different thickness. The binding energy values for Mo $3d_{5/2}$ and S $2p_{3/2}$ core levels obtained from the fits of spectra from both poly- and single crystal MoS₂ are shown in Fig. S4e. For the case of polycrystalline MoS₂, both Mo $3d_{5/2}$ and S $2p_{3/2}$ core levels show an up/down shift behavior, where 1L and 3L samples show higher binding energy compared to 2L and 4L samples and this indicates that the whole XPS spectrum has a rigid shift. For the single crystal BEs we report the weighted average of the fitting

components of the two core levels spectra shown in Fig. S4c and Fig. S4d. Single crystals MoS₂ show on average a shift towards higher binding energies from both Mo 3*d* and S 2*p* core levels spectra, see the caption of Fig. S4 for a more detailed discussion. The stoichiometry of the samples (Fig. S4f) is obtained from the S²⁻/Mo⁴⁺ total area ratio with relative sensitivity factors of 9.5 and 1.67 for Mo 3*d* and S 2*p* core levels respectively. We obtain a slightly off stoichiometry value of the S/Mo ratio of about 2.15 for all polycrystalline samples. We also report the stoichiometry obtained on the single crystals, considered as an average of the contribution from crystals of different thickness. Compared to average single crystal S/Mo ratio, polycrystalline samples show a value slightly higher than the stoichiometric one. This indicates an excess of S atoms or an abundance of Mo vacancies. A chemical ratio higher than 2 (S/Mo > 2) is generally associated to a p-type semiconducting behavior. However, n-type defects can also be present as demonstrated by the small tail present in the VB spectra close to the Fermi level (Fig. S6)⁶. This observation about stoichiometry, together with the shift towards higher energies of the binding energies of the core levels studied, suggests a lower p-doping level in the single crystal MoS₂, compared to its polycrystalline counterpart. This overall picture strongly agrees with results obtained from local KPFM experiments, where we are able to measure the work function (WF) with nanometer spatial resolution (see Fig.4c and Fig.S7-S8), obtaining WF values for single crystal MoS₂ which are lower than polycrystalline MoS₂, for each given thickness, i.e. more p-type character in polycrystalline than single crystals.

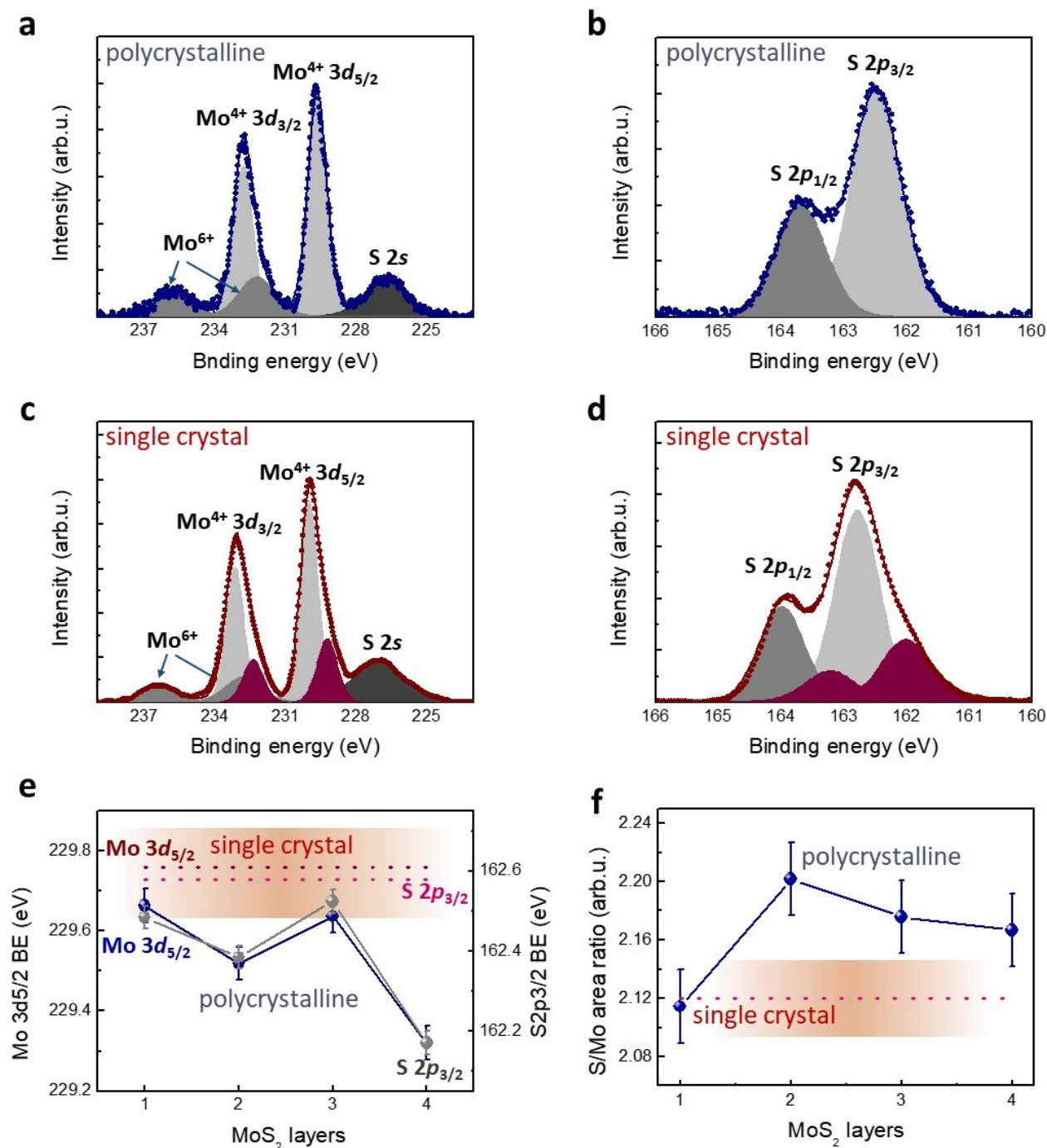


Figure S4. Mo 3d and S 2p XPS spectra of polycrystalline MoS₂. (a) Mo 3d and (b) S 2p core level spectra of 1 layer polycrystalline MoS₂. (c) Mo 3d and (d) S 2p core level spectra of single crystal MoS₂. Spectra are the result of contributions from single crystals of different thickness. (e) Binding energy from Mo 3d and S 2p core level spectra vs. number of MoS₂ layers, for polycrystalline and single crystal samples. For the single crystals we report the weighted average values between the two maxima of the fitting peaks used to fit the core levels of Mo 3d_{5/2} (dark red dashed line) and S 2p_{3/2} (violet dashed line), respectively. The weighted average is calculated with respect to the areas of the fitting peaks. The shadowed region in (e) indicates the respective standard deviations obtained from the calculation of the weighted averages. (f) XPS stoichiometry of polycrystalline and single crystal MoS₂ samples. For single crystal MoS₂, values reported are extracted from areas of the sample including crystals of different thickness, and are thus considered averaged over the number of layers. The shadowed region in panel (f) represent the average error.

The O 1s core level spectra shown in Fig. S5a is highly asymmetric because of multiple peaks deconvoluted using the fitting procedure. The lower binding energy component at about 530.0-530.8 eV corresponds to metal-oxygen bonds, which in our case can be oxygen bonded to Mo in MoO₃ or to Al in Al₂O₃ substrate. In the case of 1L MoS₂ sample shown in Fig. S5a only the Al₂O₃ component is visible. Increasing the number of MoS₂ layers, the oxygen component attributed to Al₂O₃ decreases while that one attributed to MoO₃ increases (data not shown). Furthermore, the main component at 531.5 eV corresponds to oxygen in hydroxyl OH groups. The relative concentration of the OH groups as obtained by the fitting procedure is reported in Fig. S5b. It can be observed that 1 and 3 layers of MoS₂ have the higher OH content and this indicates higher induced negative charges to compensate the dipoles at the grain boundaries. Finally, the two components at higher binding energy correspond to adsorbates from the ambient atmosphere, namely oxygen with lower coordination (at about 532.4 eV) and physisorbed and chemisorbed water at the surface (at about 533.6 eV). Since our XPS measurements are performed at room temperature and UHV pressure, weakly bonded adsorbates, as H₂O and molecular or atomic oxygen, may easily desorb⁷. For this reason, their contribution to the spectrum in Fig. S5a is very low, while the dissociated OH form is strongly bound to the surface. The interaction between hydroxyl groups and MoS₂ is considered one important source of n-type doping⁸.

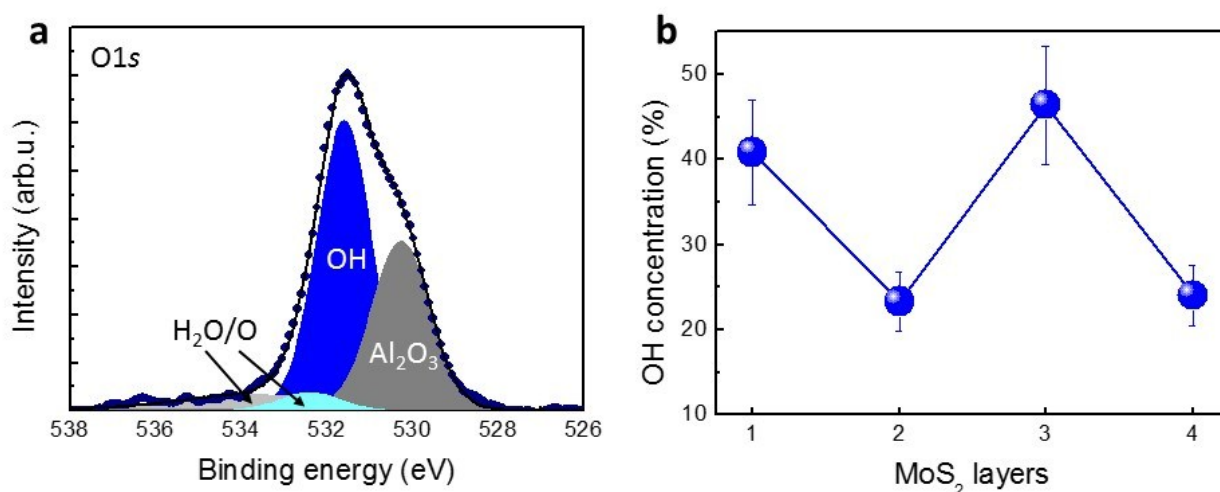


Figure S5. a) O 1s core level spectra for 1L polycrystalline MoS₂ sample. b) Hydroxyl OH concentration vs. MoS₂ thickness calculated in percent of the whole O 1s spectra.

VB spectra for 1-4 layers of polycrystalline MoS₂ are reported in Fig. S6, together with the fitting made to extrapolate the valence band maximum (VBM). The fitting is performed by the linear regression in the Mo 4d_{z2} energy region. VBM is obtained from the intersection with zero⁶. The tail observed in the VB spectra close to the Fermi level (Fig. S6) can be attributed to OH groups acting as n-type defects. Such defects are particularly evident in the odd-numbered layers and contribute to the shift of the Fermi level towards the conduction band, thus increasing the VBM and reducing the W_F.

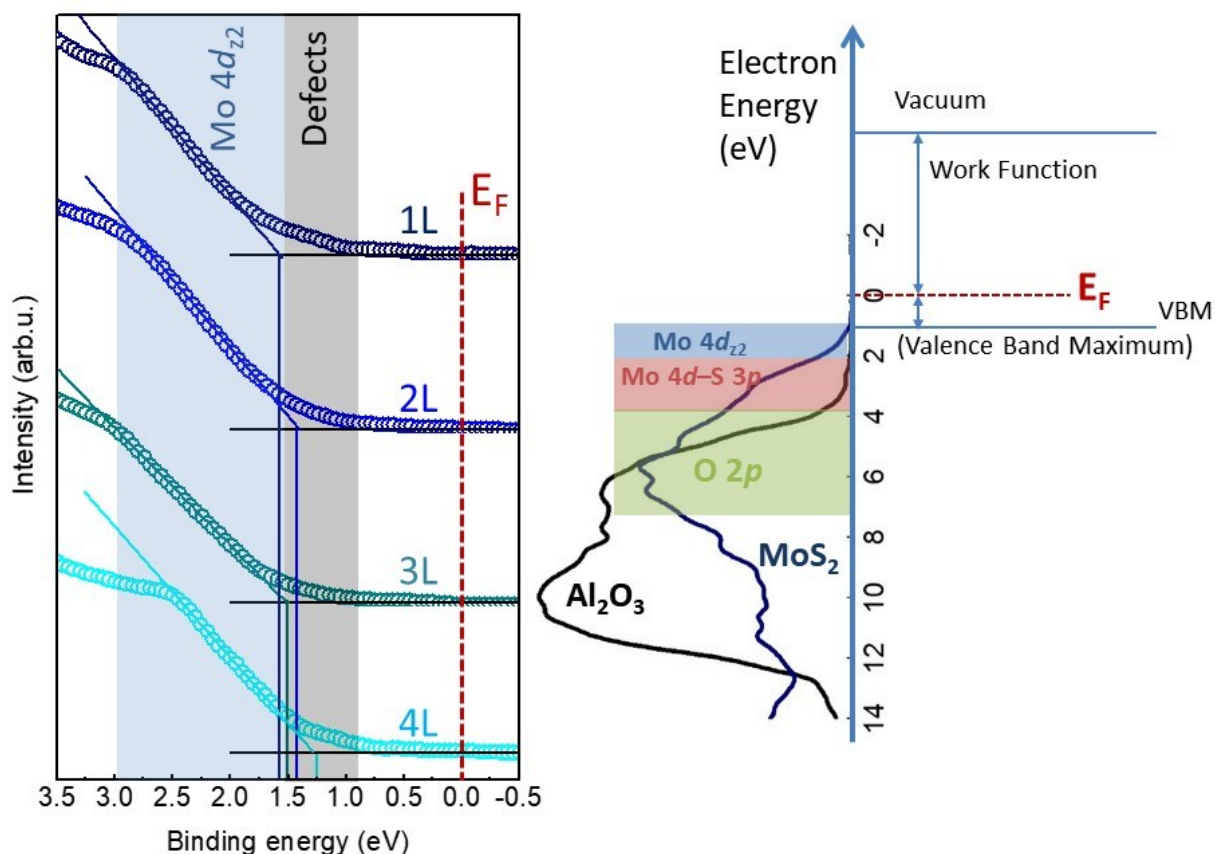


Figure S6. Procedure to obtain the valence band maximum (VBM) from XPS spectra in polycrystalline MoS₂. Left: Magnification of the Mo 4d_{z2} energy region of the valence band spectra of the four polycrystalline MoS₂ samples, with thickness from 1 to 4 layer. The straight lines are the fit made to extrapolate the valence band maximum. The tail associated to n-type defects is also highlighted. Right: Energy diagram with the valence band spectra measured for the substrate (in black) and for 1 layer MoS₂ (in blue), which is the same as the one reported in dark blue on the top of the left figure. The energy levels contributing to the valence band are highlighted, i.e. Mo 4d_{z2} band developing at ~2 eV from the VBM (blue shadowed region) and the hybridized Mo 4d and S 3p orbitals (red shadowed region) which partially overlap with O 2p orbitals of the sapphire substrate (green shadowed region).

KPFM and tapping-mode AFM imaging

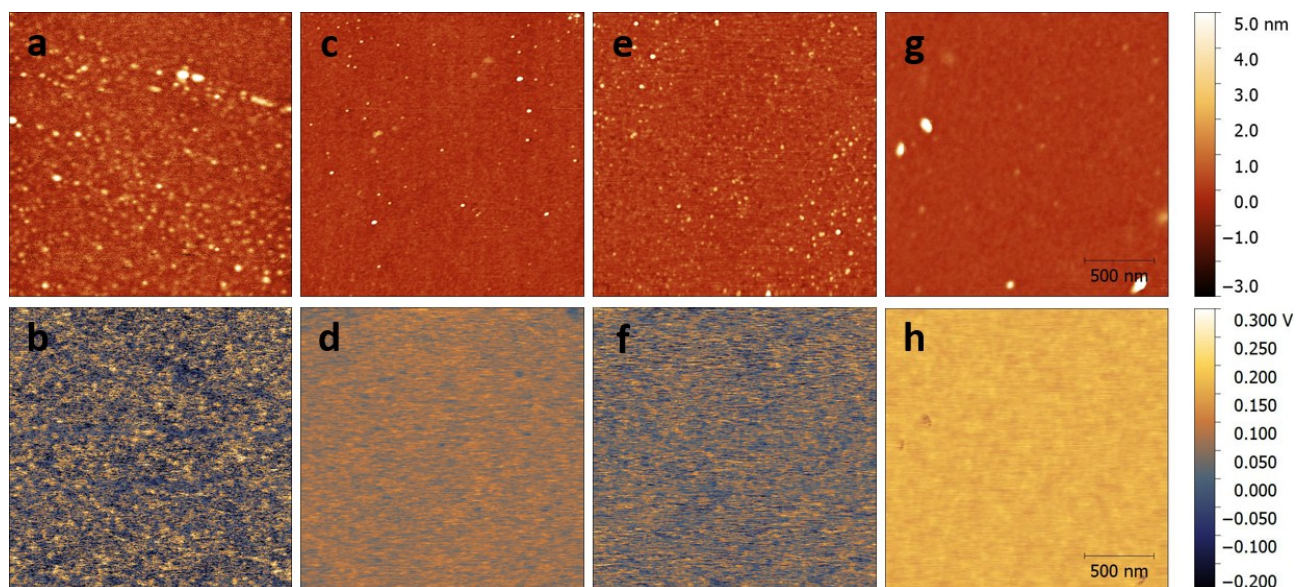


Figure S7. FM-KPFM measurements on polycrystalline MoS₂. Sequence of tapping-mode AFM topography (a, c, e, g) and FM-KPFM images (b, d, f, h) of polycrystalline samples of 1 layer (a, b), 2 layers (c, d), 3 layers (e, f) and 4 layers (g, h) MoS₂. Images size for all samples is 2 x 2 μm^2 (512 x 512 pixels). Topography images have the same vertical scale (z scale = 8 nm); same for KPFM images (here, contact potential difference (CPD) scale is 0.5 V).

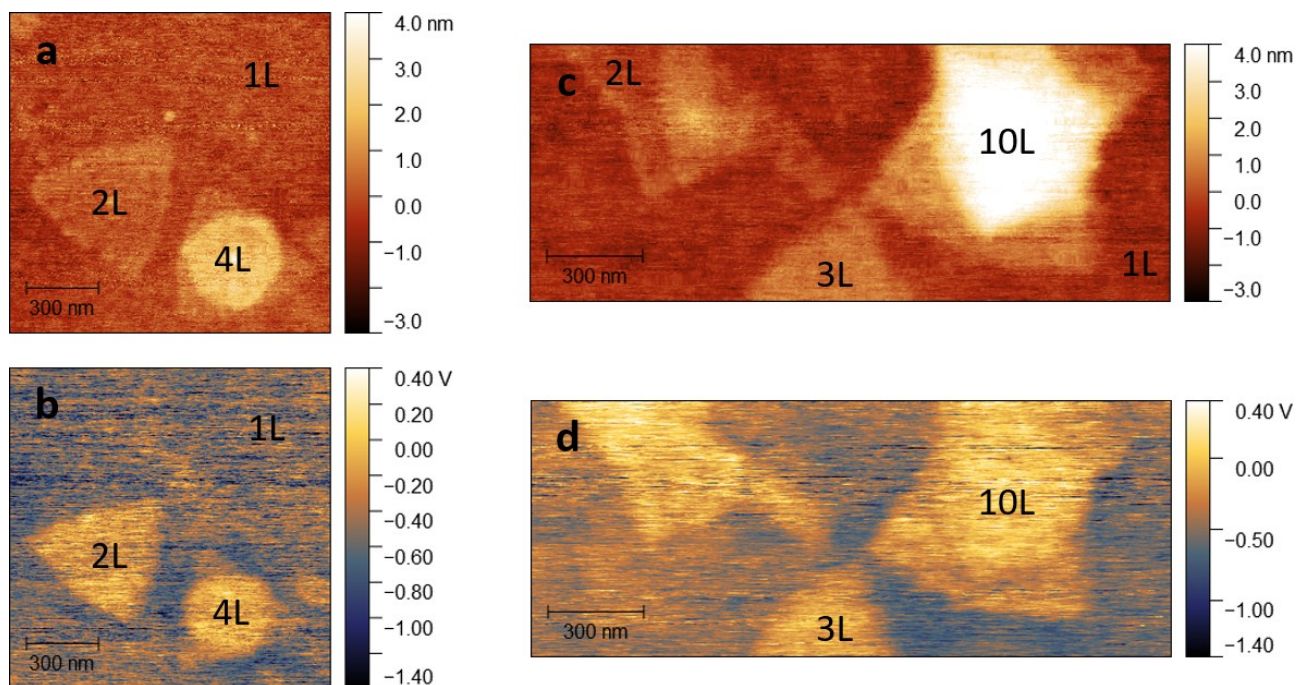


Figure S8. KPFM measurements on single crystal MoS₂. Tapping mode AFM topography (a, c) and FM-KPFM (b, d) images of single crystal MoS₂ where triangular crystals of different thickness and of size < 1 micrometer are visible. Images have 512 x 512 pixels (a, b) and 256 x 256 pixels (c, d). Topography images have the same vertical scale (z scale = 6 nm); same for KPFM images (here, CPD scale is 1.8 V).

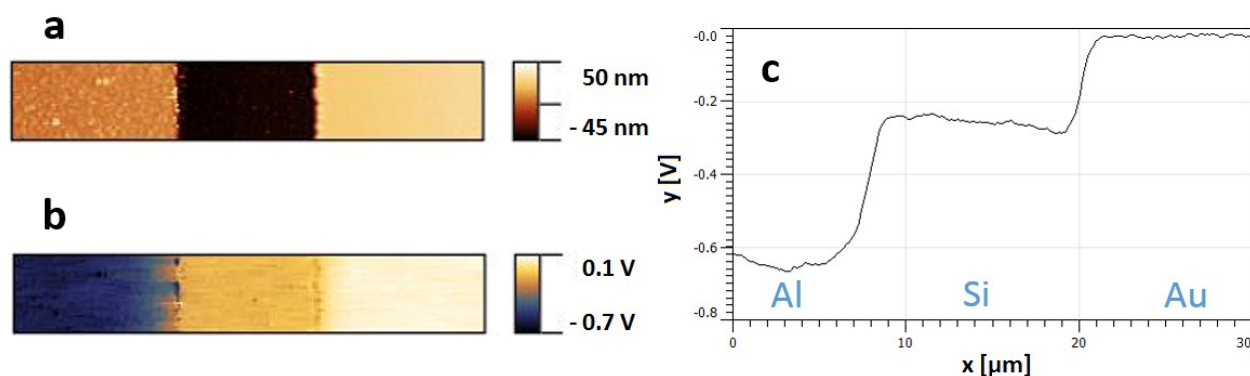


Figure S9. Calibration of the tip work function ($W_{\text{F}}^{\text{tip}}$). Tapping mode AFM (a) and FM-KPFM (b) images of a calibration sample for KPFM containing, from left to right, aluminum (Al), gold (Au) and silicon (Si) regions (PFKPFM-SMPL, Bruker). Images size is $23 \times 4 \mu\text{m}^2$. (c) Average CPD profile extracted from the image in (b). $W_{\text{F}}^{\text{tip}}$ is calculated from the value of the contact potential difference (CPD) in the gold (right) region as $W_{\text{F}}^{\text{tip}} = W_{\text{F}}^{\text{Au}} - e \cdot \text{CPD}$. We use two different tips for experiments on polycrystalline and single crystal MoS_2 . Assuming $W_{\text{F}}^{\text{Au}} = 5.1 \text{ eV}^{9, 10}$, extracted $W_{\text{F}}^{\text{tip}}$ is 5.13 eV for polycrystalline MoS_2 , and 5.03 eV for single crystal MoS_2 .

1. Yue, Q., Shao, Z.Z., Chang, S.L. & Li, J.B. Adsorption of gas molecules on monolayer MoS_2 and effect of applied electric field. *Nanoscale Research Letters* **8** (2013).
2. Butt, H.-J. & Jaschke, M. Calculation of Thermal Noise in Atomic Force Microscopy. *Nanotechnology* **6**, 1-7 (1995).
3. Carpick, R.W., Ogletree, D.F. & Salmeron, M. Lateral Stiffness: A New Nanomechanical Measurement for the Determination of Shear Strengths with Friction Force Microscopy. *Appl. Phys. Lett.* **70**, 1548-1550 (1997).
4. Liu, W., Bonin, K. & Guthold, M. Easy and Direct Method for Calibrating Atomic Force Microscopy Lateral Force Measurements. *Rev. Sci. Instrum.* **78**, 063707 (2007).
5. Riedo, E., Pallaci, I., Boragno, C. & Brune, H. The 2/3 Power Law Dependence of Capillary Force on Normal Load in Nanoscopic Friction. *J. Phys. Chem. B* **108**, 5324-5328 (2004).
6. Lin, Y.-K. et al. Thickness-Dependent Binding Energy Shift in Few-Layer MoS_2 Grown by Chemical Vapor Deposition. *ACS applied materials & interfaces* **8**, 22637-22646 (2016).
7. Shuxian, Z., Hall, W.K., Ertl, G. & Knözinger, H. X-Ray Photoemission-Study of Oxygen and Nitric-Oxide Adsorption on MoS_2 . *J. Catal.* **100**, 167-175 (1986).
8. de la Rosa, C.J.L. et al. Highly Efficient and Stable MoS_2 FETs with Reversible n-Doping Using a Dehydrated Poly (vinyl-alcohol) Coating. *Nanoscale* **9**, 258-265 (2017).
9. Kahn, A. Fermi level, work function and vacuum level. *Mater. Horiz.* **3**, 7-10 (2016).
10. Kim, J.H. et al. Work Function Variation of MoS_2 Atomic Layers Grown with Chemical Vapor Deposition: The Effects of Thickness and the Adsorption of Water/Oxygen Molecules. *Appl. Phys. Lett.* **106**, 251606 (2015).